Hybrid Numerical-Experimental Model Update Based on Correlation Approach for Turbine Components

Hybrid Numerical-Experimental Model Update Based on Correlation Approach for Turbine Components

Zeeshan Saeed*

Christian Maria Firrone

Teresa Maria Berruti

Department of Mechanical and Aerospace Engineering

Politecnico di Torino

Corso Duca degli Abruzzi 24, 10129

Turin, Italy

ABSTRACT

Bladed-disks in turbo-machines experience high cycle fatigue failures due to high vibration amplitudes. Therefore, it is important to accurately predict their dynamic characteristics including the mechanical joints at blade-disk interfaces. Before the experimental identification of these joints, it is of paramount importance to accurately measure the interface degrees-of-freedom (DoF). However, they are largely inaccessible for the measurements. For this reason, expansion techniques can be used in order to update the single components. But the expansion can be affected adversely if the measurements are not properly correlated with the updated model.

Therefore, a frequency domain expansion method called System Equivalent Model Mixing (SEMM) is used to expand a limited set of measurements to a larger set of numerical DoF. Different measured models – termed the overlay models – are taken from an impact testing campaign of a blade and a disk and coupled to the numerical model according to the SEMM. The expanded models – termed the hybrid models – are then correlated with the validation channels in a round-robin way by means of Frequency Response Assurance Criteria (FRAC). The global correlations depict whether or not a measurement and the respective expansion is properly correlated. By this approach, the least correlated channels can be done away with from the measurements to have a better updated

*Address all correspondence to this author (Email: zeeshan.saeed@polito.it)

hybrid model. The method is tested on both the structures (the blade and the disk) and it is successfully shown that removing the uncorrelated channels does improve the quality of the hybrid models.

Keywords: Bladed-disk, SEMM, Dynamic Expansion, FRAC, FRF Correlations, Model Update.

Nomenclature

Abbreviations

DoF	Degree(s) of freedom
FBS	Frequency Based Substructuring
FRAC	Frequency Response Assurance Criteria
FRF	Frequency Response Function
LDV	Laser Doppler Vibrometry
SEMM	System Equivalent Model Mixing

Symbols

$\mathbf{B}$	Signed Boolean matrix
$\mathbf{f}$	Vector of external forces
$\mathbf{g}$	Vector of interface forces
n	Number of entries or elements
$\mathbf{Y}$	FRF matrix
$\bar{\mathbf{Y}}$	Dually coupled FRF matrix
$\mathbf{u}$	Vector of displacement, velocity or acceleration DoF

Subscripts

b	Boundary DoF - physical
C	For Boolean matrix of compatibility
c	Set of DoF where compatibility is applied
E	For Boolean matrix of equilibrium
e	Set of DoF where equilibrium is applied
g	Global set of DoF
i	Set of internal DoF; Dummy index for rows of a matrix
j	Dummy index for columns of a matrix
o	Set of other / extra DoF in the numerical model

r Index for different channels in the experimental model

v Set of validation DoF for response

w Set of validation DoF for input

Superscripts

A, B Substructures A and B

AB Coupled structure AB

avg Mean of the elements

exp Experimental Model

N Numerical model

ov Overlay Model

R Removed model

r Index for different models

S Hybrid Model (Expanded or Updated)

Greek Symbols

λ Lagrange multipliers

ω Frequency in rad/s.

ϕ Frequnecy Response Assurance Criteria

1 INTRODUCTION

A mechanical component in any system should have a certain reliability that can be predicted by its different descriptions, called models. Each model can describe some of its aspects but lacks in the other. Therefore, it needs to be validated against another model. From the dynamics viewpoint, for example, a numerical model can provide a larger description of the system dynamics based on the nominal or ideal properties (geometry, material, constraints), but it may lack the characteristics of the actual component. On the other hand, an experimental model of the same may provide richer and compact information to be used for validation purposes but the testing may have been performed out of its usual service environment [1]. Besides, the measurements can only be performed on a limited set of the degrees-of-freedom (DoF) and can be prone to random noise and errors. This implies that one cannot absolutely say that one model describes the actual system in its entirety. Therefore, the two descriptions of the same component should complement each other in order to make accurate predictions.

In this context, the finite element (FE) model updating of the mechanical systems has been very popular in the last couple of decades. They minimize a residual vector of measured and predicted quantities by differentiating the sensitivity matrix with respect to the design parameters [2]. Those properties are then updated globally [3, 4] or locally. The local properties updating by the modal methods has remained quite popular for a long while in which the modal properties were extracted from the measurements c.f. [5, 6]. However, these methods fall short in cases when the modal density is high or when the

modal truncation is significant or when enough modes could not be measured affecting the predictability at higher modes. The response based methods then provide a way that does not require further estimation of the data [7, 8]. Irrespectively, the measurements can only be made at a few DoF in the system (let alone the complex systems) which limit these methods.

When the dynamic information is needed at an inaccessible DoF, the expansion methods have to be examined. In the modal domain, System Equivalent Reduction Expansion Process (SEREP) expands the measured modes to the unmeasured modes by means of a numerical modal basis [9]. The expanded modal basis can have some non-smoothness because of the measured modes. Some correlation based improvements were suggested in the method called Variability Improvement of Key Inaccurate Node Groups [10]. The investigation used statistical correlations such as Modal Assurance Criteria (MAC) and Pseudo Orthogonality Check (POC) to retain only the correlated modes. As with the modal methods, it experiences the same problems, especially the inability to accurately measure the higher modes.

In the response based measurements, an expansion technique called System Equivalent Model Mixing (SEMM) exploits different equivalent models of the same component [11]. It is based on Frequency Based Substructuring [12]. A set of FRFs over a limited DoF in a physical component is overlaid on a larger DoF in its parent numerical model. The resulting hybrid or the expanded model of the SEMM mimics the measurements and the remaining DoF are the expansion. The SEMM can be thought as the frequency domain counter-part of the SEREP. It has certain advantages over the SEREP such as: 1) modal parameters estimation is not required and hence no limitation on the closely spaced modes, 2) mode shapes need not to be measured, 3) the hybrid model is full rank. But it comes at the cost of frequency dependent response function matrices which is not significant with the modern day computing resources and the development of reduced order models.

To quantify how do the FRFs correlate with the measurements, the frequency domain correlation coefficients such as Frequency Response Assurance Criteria (FRAC) [13] are being used by the researchers. Its different variants were developed similar to the MAC [14]. A review of many modal and frequency based correlation is given in [15].

In this paper, a FRAC correlation based method is proposed to identify the uncorrelated measurement channels of an experimental model by using System Equivalent Model Mixing (SEMM). The hybrid model can be regarded as an updated numerical model of the system in which the experimental dynamics on a limited DoF set are expanded to a larger DoF set. We use different subsets of the impact testing measurements and expand them to the same numerical model. By using the FRAC, we identify the measurement channels that can be classified based on the correlation levels. This helps filter out, in a systematic way, the bad or uncorrelated channels to improve the expansion results. The case-studies are two subsystems of a blade and a disk upon which impact measurements have been performed. These components being typical of a turbine have complex geometries and inaccessible DoF; unlike many simple academic cases. The same test-case has been studied by the authors in the dynamic sub-structuring context describing in detail the specific challenges [16] .

The expanded models produced in this paper will provide a suitable basis for a further analysis, about the identification of the joint [17, 18] between the blade and disk. This will be achieved by measuring FRFs on the assembled system (blade and disk), by expanding the FRFs to the interface and by applying the substructure decoupling to identify the joint dynamic properties.

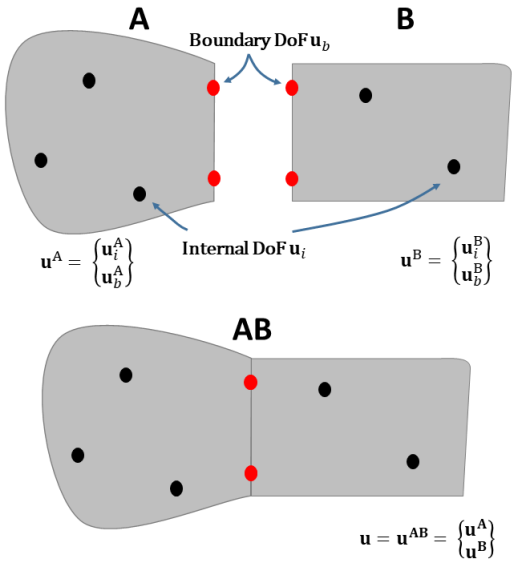

Fig. 1: The FBS coupling: the two subsructures A and B are coupled at their respective boundary DoF with rigid connections.

2 THEORETICAL AND MATHEMATICAL BACKGROUND

The theoretical basis of the System Equivalent Model Mixing (SEMM) are here briefly recapped. The SEMM is a method of constructing a hybrid model of a dynamic system based on the numerical model of the system and on measured responses only in some points of the system. The SEMM is based on Frequency Based Substructuring (FBS) which will also be briefly introduced.

2.1 FREQUENCY BASED SUB-STRUCTURING

The FBS method suggests that two adjacent substructures can be coupled in frequency domain by defining appropriate compatibility and equilibrium conditions at the interface [19]. Consider the two substructures A and B of Fig. 1 whose uncoupled equations of motion are compactly written in the admittance form as:

$$\mathbf{u} = \mathbf{Y}\,(\,\mathbf{f} + \mathbf{g}\,) \tag{1}$$

where $\mathbf{u}$, $\mathbf{f}$ and $\mathbf{g}$ are vectors of displacement DoF, external forces and interface forces of the two substructures, respectively. $\mathbf{Y}$ is the uncoupled admittance (block diagonal) matrix.

$$\mathbf{Y} = \begin{bmatrix} \mathbf{Y}^{\mathrm{A}} & \\ & \mathbf{Y}^{\mathrm{B}} \end{bmatrix} \tag{2}$$

The explicit frequency dependence has been omitted. The two substructures are coupled at their corresponding boundary

DoF $\mathbf{u}_b$.

In order to do that, the Lagrange multipliers λ at the interface forces $\mathbf{g}$ are introduced such that $\mathbf{g} = -\mathbf{B}^T\lambda$ and substituted in Eqn. (1). The substitution satisfies the equilibrium as $\mathbf{B}$ is a *signed* Boolean matrix that picks the appropriate boundary DoF. The compatibility can then be applied by the following set of equations called the dual formulation [12].

$$\begin{aligned} \mathbf{u} &= \mathbf{Y}\,(\,\mathbf{f} - \mathbf{B}^T\lambda\,) \\ \mathbf{B}\mathbf{u} &= \mathbf{0} \end{aligned} \tag{3}$$

By simple algebraic steps, Eqn. (3) can be solved to yield a single line expression for the Lagrange Multiplier Frequency Based Substructuring (LM-FBS), i.e.

$$\mathbf{u} = \mathbf{Y}\mathbf{f} - \mathbf{Y}\mathbf{B}^T(\mathbf{B}\mathbf{Y}\mathbf{B}^T)^{-1}\mathbf{B}\mathbf{Y}\mathbf{f} \quad \Rightarrow \quad \mathbf{u} = \mathbf{Y}^{\mathrm{AB}}\mathbf{f} \tag{4}$$

$$\mathbf{Y}^{\mathrm{AB}} = \mathbf{Y} - \mathbf{Y}\mathbf{B}^T(\mathbf{B}\mathbf{Y}\mathbf{B}^T)^{-1}\mathbf{B}\mathbf{Y} \tag{5}$$

The coupled matrix $\mathbf{Y}^{\mathrm{AB}}$ consists of FRFs of all the DoF of the substructures including the interface ones.

The FBS framework also provides a convenient way to decouple a substructure from the coupled or assembled structure. Fictitious admittances are used to decouple the substructure. However, in this case the interface does not necessarily have to be only at the boundary DoF, it may include the internal DoF of the substructures. The so-called extended interface is constructed by defining the Boolean matrices separately for compatibility DoF $\mathbf{B}_C$ and equilibrium DoF $\mathbf{B}_E$. For instance, if one wants to decouple substructure A from the coupled structure AB to identify the dynamics of substructure B, the uncoupled admittance is expressed as

$$\mathbf{Y} = \begin{bmatrix} \mathbf{Y}^{\mathrm{AB}} & \\ & -\mathbf{Y}^{\mathrm{A}} \end{bmatrix} \tag{6}$$

and substituted in Eqn. (5) with $\mathbf{B}_C$ and $\mathbf{B}_E$ to find

$$\bar{\mathbf{Y}}^{\mathrm{B}} = \mathbf{Y} - \mathbf{Y}\,\mathbf{B}_E^T\,(\mathbf{B}_C\mathbf{Y}\,\mathbf{B}_E^T)^{+}\,\mathbf{B}_C\mathbf{Y} \tag{7}$$

where $(\bullet)^+$ is the generalized inverse. $\bar{\mathbf{Y}}^{\mathrm{B}}$ has all the DoF in $\mathbf{Y}^{\mathrm{AB}}$ and $\mathbf{Y}^{\mathrm{A}}$. Only the independent entries are required to obtain $\mathbf{Y}^{\mathrm{B}}$. Note that the coupling (or decoupling) in Eqn. (5) and (7) is rigid which means that compatibility and the equilibrium are exactly satisfied.

2.2 System Equivalent Model Mixing

The System Equivalent Model Mixing (SEMM) method is an expansion technique based on the FBS framework that takes different equivalent models of the same structure and couples them so that the dynamics of one are overlaid on the other. It relies on three models, namely, an overlay, a parent and a removed model. In [11], its different interface formulations are presented. A recap of the models used in the SEMM extended interface formulations is given below.

2.2.1 Overlay Model

It is a model in the SEMM terminology whose dynamics are important and should be imposed on another model. In the practical application of SEMM, this overlay model is a model which collects experimental results. Let us denote an experimental representation of the structure, in the form of FRFs as $\mathbf{Y}^{\mathrm{exp}}$. This can include FRFs where the response and the force are along the same DoF (drive-point FRFs) and FRFs where the response and the force are along different DoF (transfer FRFs). It is well-known that accurately measuring drive-point FRFs can become very challenging. Besides, the measured DoF or channels in an experimental model are always limited in number. Hence, the DoF structure is defined as:

$$\begin{Bmatrix} \mathbf{u}_c \\ \mathbf{u}_v \end{Bmatrix}^{\mathrm{exp}} = \mathbf{Y}^{\mathrm{exp}}\,\mathbf{f}^{\mathrm{exp}} = \begin{bmatrix} \mathbf{Y}_{ce} & \mathbf{Y}_{cw} \\ \mathbf{Y}_{ve} & \mathbf{Y}_{vw} \end{bmatrix}^{\mathrm{exp}} \begin{Bmatrix} \mathbf{f}_e \\ \mathbf{f}_w \end{Bmatrix}^{\mathrm{exp}} \tag{8}$$

where $\mathbf{u}^{\mathrm{exp}}$ represents all the DoF where the response could be measured. The measured $\mathbf{u}_c^{\mathrm{exp}}$ channels will be later used as compatibility DoF (between the numerical and the experimental model) and $\mathbf{f}_e^{\mathrm{exp}}$ as equilibrium DoF (where loads are experimentally applied) in the SEMM coupling. $\mathbf{u}_v^{\mathrm{exp}}$ and $\mathbf{f}_w^{\mathrm{exp}}$ are sets of validation channels and validation input channels, respectively, which will not be used in the expansion (model update) process. Instead they are used to validate the expanded FRFs. The choice of subscripts emphasizes that $\mathbf{Y}^{\mathrm{exp}}$ is an overdetermined set, however, it is not restricted to this form. From this experimental model $\mathbf{Y}^{\mathrm{exp}}$, a subset is taken as an overlay model.

$$\mathbf{u}_c^{\mathrm{ov}} = \mathbf{Y}^{\mathrm{ov}}\,\mathbf{f}_e^{\mathrm{ov}} \quad \text{where} \quad \mathbf{Y}^{\mathrm{ov}} = \mathbf{Y}_{ce}^{\mathrm{exp}} \tag{9}$$

The size of $\mathbf{Y}^{\mathrm{ov}}$ is $n_c \times n_e$. This model is overlaid on the parent model to be described next.

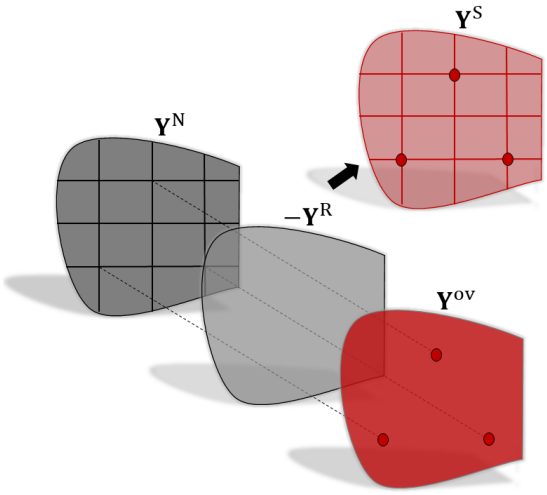

Fig. 2: Equivalent models of the substructure A of Fig. 1: The parent numerical model $\mathbf{Y}^{\mathrm{N}}$ has the essential DoF. Its own dynamics are decoupled by the removed model $\mathbf{Y}^{\mathrm{R}}$ and coupled by $\mathbf{Y}^{\mathrm{ov}}$. The resulting hybrid or expanded model $\mathbf{Y}^{\mathrm{S}}$ mimics at the corresponding overlay model's DoF.

2.2.2 Parent Model

The overlay model has only a limited number of DoF. An equivalent numerical model of the same system can provide a larger set of DoF upon which the overlay model's dynamics can be expanded. A full finite element (FE) model or its reduced order model (ROM) in the admittance form is used as a numerical parent model in the SEMM method. The parent model's DoF set, referred to as global DoF $\mathbf{u}_g$, can thus be categorized as follows:

$$\mathbf{u}_g^{\mathrm{N}} = \begin{Bmatrix} \mathbf{u}_c \\ \mathbf{u}_e \\ \mathbf{u}_o \end{Bmatrix}^{\mathrm{N}} \quad \text{with} \quad \mathbf{u}_o^{\mathrm{N}} = \begin{Bmatrix} \mathbf{u}_v \\ \mathbf{u}_b \end{Bmatrix}^{\mathrm{N}} \tag{10}$$

and its admittance $\mathbf{Y}^{\mathrm{N}}$ is expressed as:

$$\mathbf{Y}^{\mathrm{N}} = \mathbf{Y}_{gg}^{\mathrm{N}} = \begin{bmatrix} \mathbf{Y}_{cc} & \mathbf{Y}_{ce} & \mathbf{Y}_{co} \\ \mathbf{Y}_{ec} & \mathbf{Y}_{ee} & \mathbf{Y}_{eo} \\ \mathbf{Y}_{oc} & \mathbf{Y}_{oe} & \mathbf{Y}_{oo} \end{bmatrix}^{\mathrm{N}} \tag{11}$$

By coupling the overlay model to this model, the unmeasured DoF can be expanded including the drive-point FRFs. This expansion involves removing parts of the numerical model (parent model) and replacing them with parts of the experimental model (overlay model). The part of the admittance removed will be called $\mathbf{Y}^{\mathrm{R}}$, the corresponding experimental admittance

that replaces it will be called $\mathbf{Y}^{\text{ov}}$. This expansion procedure will produce a "Hybrid model" as it is explained in detail in the next section.

2.2.3 Hybrid Model

The hybrid model $\mathbf{Y}^{\text{S}}$ is obtained by coupling the overlay model with the parent model and decoupling at the same time the removed model. Mathematically, using the aforementioned equivalent models, the uncoupled admittance matrix

$$\mathbf{Y} = \begin{bmatrix} \mathbf{Y}^{\text{N}} & & \\ & -\mathbf{Y}^{\text{R}} & \\ & & \mathbf{Y}^{\text{ov}} \end{bmatrix} \tag{12}$$

the appropriate signed Boolean matrices

$$\mathbf{B}_C = \begin{array}{c} \begin{matrix} \mathbf{u}_c^{\text{N}} & \mathbf{u}_e^{\text{N}} & \mathbf{u}_o^{\text{N}} & \mathbf{u}_c^{\text{R}} & \mathbf{u}_e^{\text{R}} & \mathbf{u}_o^{\text{R}} & \mathbf{u}_c^{\text{ov}} \end{matrix} \\ \left[\begin{array}{ccc|ccc|c} -\mathbf{I} & \mathbf{0} & \mathbf{0} & \mathbf{I} & \mathbf{0} & \mathbf{0} & \mathbf{0} \\ \mathbf{0} & -\mathbf{I} & \mathbf{0} & \mathbf{0} & \mathbf{I} & \mathbf{0} & \mathbf{0} \\ \mathbf{0} & \mathbf{0} & -\mathbf{I} & \mathbf{0} & \mathbf{0} & \mathbf{I} & \mathbf{0} \\ \mathbf{0} & \mathbf{0} & \mathbf{0} & -\mathbf{I} & \mathbf{0} & \mathbf{0} & \mathbf{I} \end{array}\right] \end{array} \tag{13}$$

$$\mathbf{B}_E = \begin{array}{c} \begin{matrix} \mathbf{f}_c^{\text{N}} & \mathbf{f}_e^{\text{N}} & \mathbf{f}_o^{\text{N}} & \mathbf{f}_c^{\text{R}} & \mathbf{f}_e^{\text{R}} & \mathbf{f}_o^{\text{R}} & \mathbf{f}_e^{\text{ov}} \end{matrix} \\ \left[\begin{array}{ccc|ccc|c} -\mathbf{I} & \mathbf{0} & \mathbf{0} & \mathbf{I} & \mathbf{0} & \mathbf{0} & \mathbf{0} \\ \mathbf{0} & -\mathbf{I} & \mathbf{0} & \mathbf{0} & \mathbf{I} & \mathbf{0} & \mathbf{0} \\ \mathbf{0} & \mathbf{0} & -\mathbf{I} & \mathbf{0} & \mathbf{0} & \mathbf{I} & \mathbf{0} \\ \mathbf{0} & \mathbf{0} & \mathbf{0} & \mathbf{0} & -\mathbf{I} & \mathbf{0} & \mathbf{I} \end{array}\right] \end{array} \tag{14}$$

are substitued in Eqn. (7) to get dually coupled admittance $\bar{\mathbf{Y}}$ which is then reduced to the primal DoF by the following transformation:

$$\mathbf{Y}^{\text{S}} = (\mathbf{L}_C)^{+}\, \bar{\mathbf{Y}}\, (\mathbf{L}_E^{T})^{+} \tag{15}$$

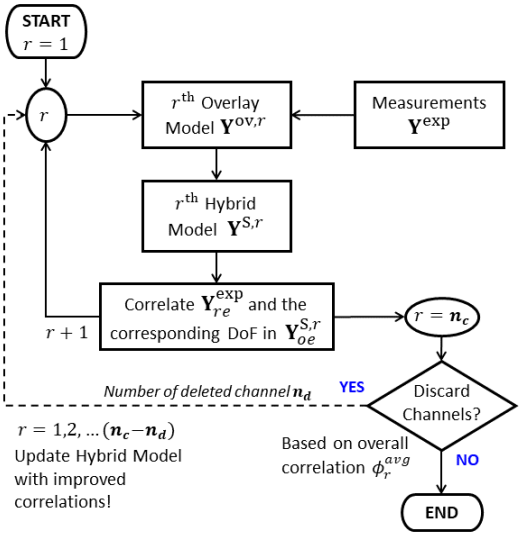

Fig. 3: The process flow of the method to identify the response channel.

The localisation matrices $\mathbf{L}_C$ and $\mathbf{L}_E$ can be obtained by calculating the nullspace of respective $\mathbf{B}_C$ and $\mathbf{B}_E$. A single-line expression is then derived as [20]:

$$\mathbf{Y}^{\text{S}} = \mathbf{Y}_{gg}^{\text{N}} - \mathbf{Y}_{gg}^{\text{N}} \left(\mathbf{Y}_{cg}^{\text{N}}\right)^{+} \left(\mathbf{Y}_{ce}^{\text{N}} - \mathbf{Y}_{ce}^{\text{ov}}\right) \left(\mathbf{Y}_{ge}^{\text{N}}\right)^{+} \mathbf{Y}_{gg}^{\text{N}} \tag{16}$$

The procedure is schematically shown in Fig. 2. From the figure and Eqn. (16) the following remarks can be made:

1. The hybrid model $\mathbf{Y}^{\text{S}}$ has the same DoF structure as the parent numerical model $\mathbf{Y}^{\text{N}}$.
2. The pseudo inverses $(\mathbf{Y}_{cg}^{\text{N}})^{+}$ and $(\mathbf{Y}_{ge}^{\text{N}})^{+}$ define the extended SEMM interface through which the overlay dynamics are transmitted to the numerical model.
3. The dynamics of $\mathbf{Y}_{ce}^{\text{ov}}$ are exactly imposed on the corresponding elements of $\mathbf{Y}_{ce}^{\text{N}}$ in the absence of the SVD filters.
4. For the remaining blocks of $\mathbf{Y}^{\text{S}}$, the FRFs are expansions including the drive-point FRFs which otherwise would have been very difficult to acquire.
5. This formulation uses the extended interface formulation, and therefore, is dominated by the modes of the overlay model even at the expanded DoF.
6. The experimental FRFs in $\mathbf{Y}_{ce}^{\text{ov}}$ have not been inverted during the process; yet any noise in the experimental model is transmitted to the hybrid model.
7. The difference $|\mathbf{Y}_{ce}^{\text{N}} - \mathbf{Y}_{ce}^{\text{ov}}|$ is the expansion error and, of course, depends on the closeness between the two models.

In the next section, an experimental validation will be carried out about how the dynamic response of the system is well captured by the hybrid model in those degrees of freedom that are not included in the overlay model.

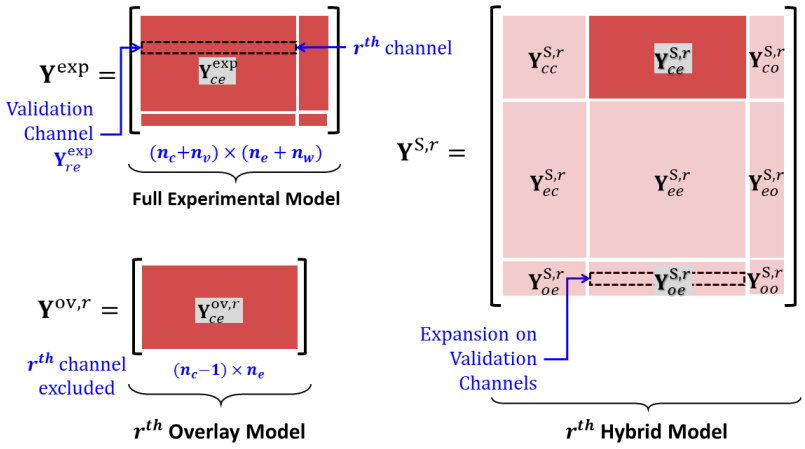

Fig. 4: An illustration of the experimental, overlay and hybrid models. The r^{th} overlay model $\mathbf{Y}^{\text{ov},r}$ is short of the r^{th} channel in experimental model $\mathbf{Y}^{\text{exp}}$. The expansion on the same DoF in the hybrid model $\mathbf{Y}^{\text{S},r}$ is obtained and then the two are correlated. The respective channels for the correlation are indicated for both $\mathbf{Y}^{\text{exp}}$ and $\mathbf{Y}^{\text{S},r}$.

3 IDENTIFYING MEASUREMENT CHANNELS BY FRF BASED CORRELATION METRICS

A critical issue in the case of measurements for identification, for example identification of a joint in a system composed of a blade connected to a disk, is that the accelerometers cannot be placed directly on the joint. Furthermore it is very difficult to measure drive-point FRFs (i.e. FRFs where the DoF of the excitation and the response are the same). It is therefore necessary to estimate the FRF of the system at locations not directly accessible and therefore not measurable. To obtain these FRFs in this paper, it is proposed to use a hybrid model as described in Section 2.2.3. As mentioned before, on the *ce* DoF of the hybrid model, the dynamics are exactly overlaid, while for the remaining DoF it is an expansion. During the measurement campaign described in this paper, one or more channels were left as reference, they will be called "validation channels" $\mathbf{u}_v^{\text{exp}}$. These validation channels were not included in the overlay model and, as a consequence, in the construction of the Hybrid model. Their measurement can then be used as reference for the validation of the predicted FRFs. The comparison between the experimental FRF and the FRF predicted by the Hybrid model is carried out through the Frequency Response Assurance Criteria (FRAC) [13].

$$\phi_{ij} = \frac{|\mathbf{Y}^{\text{S}}_{ij}(\omega)\ \mathbf{Y}^{\text{exp}*}_{ij}(\omega)|^2}{\mathbf{Y}^{\text{S}}_{ij}(\omega)\ \mathbf{Y}^{\text{S}*}_{ij}(\omega).\ \mathbf{Y}^{\text{exp}}_{ij}(\omega)\ \mathbf{Y}^{\text{exp}*}_{ij}(\omega)} \tag{17}$$

where $\mathbf{Y}^{\text{S}}_{ij}(\omega)$ and $\mathbf{Y}^{\text{exp}}_{ij}(\omega) \in \mathbb{C}^{n_\omega \times 1}$ for each i and j and $(\bullet)^*$ represents the complex conjugate. The correlation ϕ_{ij} thus determined is a number between 0 for no correlation and 1 for a strong correlation.

3.1 Identify Response Channels

It must also be highlighted that in impact testing for identification measurements, the number of response DoF by the accelerometers is limited by two factors: number of available channels in the data acquisition system and the sensor loading effect, since each accelerometer adds a mass to the system. Even if the sensors are small and the mass loading effect can be neglected, still there is a limit in the number of available channels. Therefore, a set of good or well correlated measurements is much desired to build a reliable hybrid model. In the following sections, "a posteriori" analysis on a set of experimental measurements will be performed to find the contribution of the different measurement channels. In particular, the method explained in Fig. 3 will be used to assess whether there are experimental FRFs that can be discarded in the reconstruction of the response at a certain DoF. Given a set of experimental FRFs, the FRAC is used to identify which are the most influential measurements to be included in the construction of the hybrid model. A round-robin approach for measurement channels is proposed. The process depicted in the flowchart of Fig. 3 can be explained in the following steps.

1. Define an overlay model such that one response channel is excluded from it. As depicted in Fig. 4, a row of the FRFs has been removed (top-left r^{th} channel for validation).

$$\mathbf{Y}^{\text{ov},r} \subset \mathbf{Y}^{\text{exp}} : \ \mathbf{Y}_{re}^{\text{exp}} \notin \mathbf{Y}^{\text{ov},r} \tag{18}$$

   where $r = 1, 2, ..., n_c$. The size of $\mathbf{Y}^{\text{ov},r}$ is $(n_c - 1) \times n_e$. The channel $\mathbf{Y}_{re}^{\text{exp}}$ is termed as the validation channel and is graphically illustrated in Fig. 4.
2. Perform expansion by the SEMM method with $\mathbf{Y}^{\text{ov},r}$ as per Eqn. (16) to get $\mathbf{Y}^{\text{S},r}$.
3. Correlate the corresponding r^{th} expanded channel in $\mathbf{Y}^{S,r}$ with $\mathbf{Y}_{re}^{\text{exp}}$ along all the input channels, per Eqn. (17). At each r, the correlation ϕ_r is a row which can be viewed as such indicating correlation at individual input channel or it can be averaged indicating the overall correlation level.

$$\phi_r^{\text{avg}} = \frac{1}{n_e} \sum_{j=1}^{n_e} \phi_{rj} \tag{19}$$

   Physically, it can be interpreted as how well all the channels except the r^{th} could observe the same DoF when expanded.
4. The process is repeated for all the remaining channels in a round-robin way, i.e. every channel (row) in $\mathbf{Y}_{ce}^{\text{ov},r}$ is excluded from the r^{th} overlay model upto $r = n_c$.
5. The low correlated *response channels* are identified based on the lowest correlation in Eqn. (19).

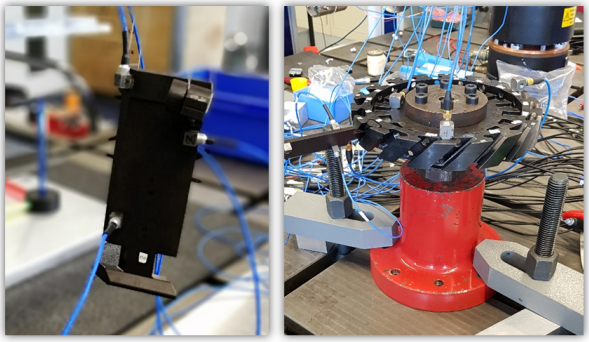

Fig. 5: The measurement setup: the blade (left) hanged with rubber mounts and the disk (right) constrained at the center with a flange.

Table 1: LIST OF THE MEASUREMENT CHANNELS ON BLADE AND DISK

Description		Blade	Disk
Measured Response Channels		15	15
Response Channels for Expansion	n_c	12	14
Response Channel Labels		(4 to 15)	(2 to 15)
Input Channels for Expansion	n_e	18	19
Input Channels Labels		(1 to 18)	(1 to 19)

4 RESULTS

In this section, the experimental activity is described to verify 1) if the hybrid model is suitable to estimate the dynamic response of a system at certain points by performing experimental measurements at other points and 2) if some uncorrelated measurements can be discarded in the construction of the hybrid model.

As a first case, the hybrid model is built for a single unconstrained ”free-free” blade (see Fig. 5 on the left) where the numerical and experimental models FRFs are in good agreement with each other. As a second case, the hybrid model is built for a more complex system: a disk constrained by a flange at its centre (see Fig. 5 on the right). In this case, the importance of starting from a well-defined numerical model to construct the hybrid model is highlighted. The choice of these particular boundary conditions was made since we need two hybrid models i) disk connected to its support and ii) blade (unconstrained) in the future perspective of using them in the sub-structuring procedure to identify the joint between the blade and disk.

In both the experimental setups, some response channels are always not used to construct the hybrid model, i.e. at least one of them is always reserved for validation: the validation consists in comparing the FRF of a channel used for validation with the FRF predicted by the hybrid model along the same degree of freedom. This may be desired for predicting the response at a particular DoF of interest. These channels and their numbers on both the components are listed in Tab. 1.

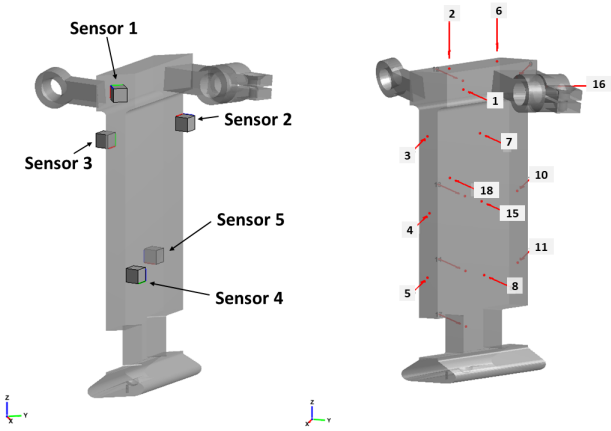

Fig. 6: The measurement setup for the blade. Each sensor has three response channels (left). All three channels of Sensor 1 are set as the validation channels. Some of the impact locations are shown in the right figure.

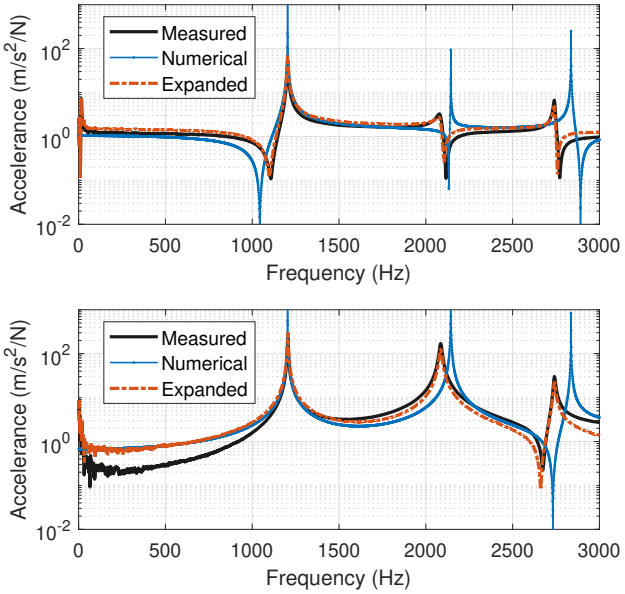

Fig. 7: FRFs of the blade at one of the validation channels in the axial direction (channel 3). For the top FRF, the blade is excited at point 6 (see Fig. 6) and for the bottom FRF, it is excited at point 17 (not visible in Fig. 6, as it is on the opposite side of the shown surface)

.

4.1 Blade

The blade depicted in Fig. 6 made of steel was hung on rubber bands, as shown in Fig. 5, to obtain the free-free constrain condition. Five triaxial accelerometers (connected to 15 response channels) are positioned along the blade and 18 points are chosen as excitation points to be hit by the instrumented hammer. An example of the obtained FRFs in Fig. 7 shows well separated modes. The FRFs (above and below) refer to the same response channel but with a different excitation point. In both the figures of Fig. 7, it can be noticed that the numerical model does not have any damping. On the contrary the hybrid model's response is damped and for most of the part, it follows the measurement, especially around the resonances. By using

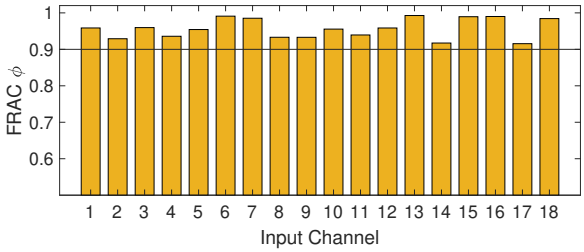

Fig. 8: Bar plot for the FRAC of the response channel 3 for all input force channels. The overall correlation is above 0.9.

Table 2: OVERALL MEAN FRAC VALUES FOR THE BLADE

Description	FRAC
With All Channels	0.947
Without Channel 4	0.967

the FRAC correlation explained in section 3, the FRFs of the "validation channels" can be compared with the hybrid model FRF on the same channel.

In Fig. 8, it is plotted the FRAC between the FRF measured on channel 3, kept as validation channel, and the FRFs predicted by the hybrid model in the same point and direction of the response in channel 3. In detail each bar represents the FRAC between the experimental FRF and the same FRF predicted by the hybrid system using all the other measurement channels (except the 3) and at each excitation (input channel). It can be noted that the FRAC values are all close to 1 for all the input channels. The FRAC for the FRFs in the top part of Fig. 7 is 0.99 (input channel 6) and for the bottom part is 0.91 (input channel 17). This is an index that tells us that the hybrid model seems to work well for estimating the FRF in points whose measures are not included in the model itself. We now want to verify whether this is true not only for the degree-of-freedom selected here (channel 3) but also for other degrees-of-freedom of the blade corresponding to other response channels.

4.1.1 Identify Uncorrelated Response Channels

As per the procedure outlined in Section 3, different overlay models are made as subset of the experimental model and then the hybrid models are generated which contain the expanded FRFs. The correlations thus obtained on each channel or DoF are shown in Fig. 9. Each curve of different colour represents the FRAC referring to each validation channel r^{th} as a function of the input channels (excitation points). Recalling Tab. 1 for the blade, note that the legend of the figure starts from the fourth channel and not the first it means that same labeled channel is used as a validation channel. Whereas the single colour of the lines shows the correlation at each input channel. It can be observed that all validation channels, except the 4th channel, have a FRAC close to 1. This means that the FRFs predicted by the hybrid model give good results for all the DoF

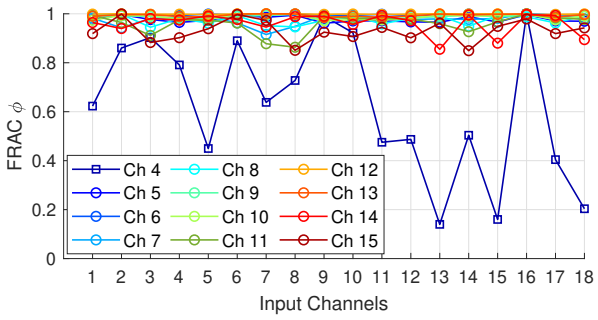

Fig. 9: Line plot of FRAC for r^{th} channel which becomes the moving reference channel at the r^{th} sequence. For example of channel 4, the plot should be read as correlation of channel 4's observability when all other channels tried to observe it.

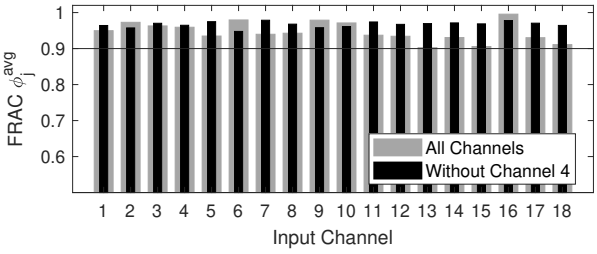

Fig. 10: FRAC bar plot vs input force channels with and without the poorly correlated response channel 4.

considered except for the DoF measured by channel 4.

The reason of this poor behaviour of channel 4 could be that the experimental response levels (for different excitation force) measured at channel 4 are too low to be observed. To verify this, the response levels at channel 4 were compared with the responses of the other channels in the same direction. It turned out that the response levels were quite low for channel 4 except where the correlation is high, for instance, input channel 9 and 16 (see Fig. 9, line with square markers for channel 4).

Due to this reason, channel 4 is to be removed by deleting the corresponding row in the *experimental model*. The corresponding DoF can either be kept as such in the parent numerical model or be deleted. To see whether or not channel 4 was an under performer, the procedure of Section 3 is repeated with one less measured channel. In Fig. 10, the average FRAC of all the FRFs (averaged at all response DoF) is plotted versus the input channels. The gray bars represent the case in which all the measured FRFs are kept in the calculation of the hybrid models, the black bars represent the case in which the FRFs measured by channel 4 are excluded in the construction of the hybrid models. It can be seen that in most cases the black bars are higher than the gray bars. This means that the set of measurements without the FRFs obtained with channel 4 leads to hybrid models that better approximate (FRAC closer to 1) the dynamics of the structure. This is also confirmed by a FRAC number computed as the average of the averages on all channels. This overall FRAC is listed in Table 2 for the case "All channels" and the case "Without channel 4". The FRAC number for the case "Without channel 4" closer to 1 than the FRAC of the case "All Channels". This observation provides a warning: in the case of construction of a hybrid model with the SEMM technique, some measured responses with small amplitude and noise can worsen the dynamic responses. It can, therefore, be decided to exclude them from the construction of the hybrid model by the proposed method.

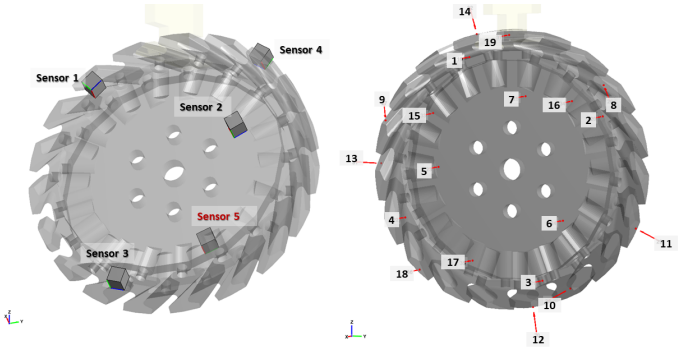

Fig. 11: The measurement setup for the disk. Each sensor has three response channels (left). Only one channel of Sensor 1 is reserved as the validation channels. Some of the impact locations are also shown (right).

4.2 Disk

The same expansion method is applied to the disk mechanical component shown in Fig. 5 (left). It is a disk with 18 slots in order to host 18 blades as the one used in the previous test-case. The disk is rigidly constrained to the ground in the centre by means of a bolted joint. Hammer tests were performed in 19 different locations (Input Channels) as already mentioned in Tab. 1 and shown in Fig. 11 (right). Five tri-axial accelerometers were used (Fig. 11 – left) to collect the disk response for a whole set of 15 Response Channels. The parent numerical model of the disk is generated from the reduced order model (Hurty-Craig-Bampton) of its full 360^o FE model.

A typical experimental response is shown in Fig. 12 (solid black line). It is possible to see how the response is definitively more complex than the one obtained for the blade as the level of modal density for a wide frequency bandwidth. In the same figure (Fig. 12 top), the calculated forced response of the corresponding FE model is shown for two different Young's moduli: the dotted line (label: 'Model 1') is obtained with a nominal value of the Young's modulus while the dash-dotted curve (label: 'Model 2') is obtained by changing the Young's modulus in order to have resonance peaks closer to the experimental resonance peaks. However, for both calculated responses, it is possible to see that the parent models produce forced responses that are far from the one of the overlay model. The main reason is to be associated to the lack of cyclic symmetry for the actual disk and the constraint, while in the FE models the cyclic symmetry property is nominally guaranteed by a cyclic geometry and constraints. The constraint modelling also remains a challenge both numerically and experimentally [21]. Response Channels from 2 to 15 are used for the model expansion by SEMM method of both numerical models and an example of the final response after expansion is shown in Fig. 12 bottom where the Response Channel 1 is used for validation. It is possible to see that the expanded model 2 FRF matches better than that of the expanded model 1 with the measured response.

By using the correlation approach, the average FRAC values according to Equation 18 are plotted in the bar plot of Fig. 13 for the two expanded models. Each bar represents how well the validation channel is reconstructed by all the other response channels. The average of the bar values is calculated and shown in Tab. 3 (With all channels) in order to give a global index of the expansion goodness and the model 2 gives better global correlation (and better model update). In order to improve the result of the correlation calculated for model 2, Response Channel 3 can be removed in the experimental model and the expansion procedure since this channel gives the worst correlation. Similarly, Response Channel 6 can be done away

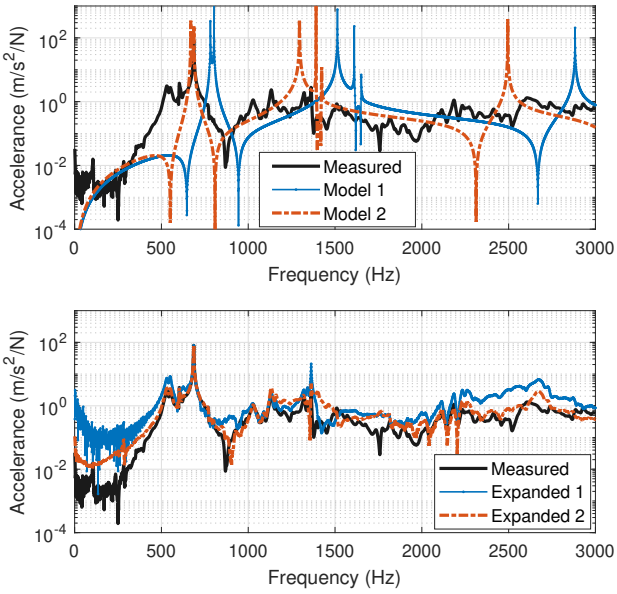

Fig. 12: Disk FRF at channel 4 (sensor 2) excited at the input channel 10: Two different numerical parent models of the disk are plotted (top). The corresponding hybrid models (bottom) are also shown. The FRF of the model 2 has higher correlation with the measurement.

with for model 1. The result is an improvement of the global FRAC index of Tab. 3 for the respective models for which these actions were made and vice versa the global FRAC index decreases when a Response Channel associated to a good correlated channel is removed.

4.3 Effect of Sensor Mass Loading

As previously mentioned, the sensors used for response measurement are triaxial accelerometers. They were preferred over more sophisticated non-intrusive measurement equipment, such as laser doppler vibrometry (LDV) [22, 23] for the different reasons listed below.

1. It is very difficult to obtain accurate measurements by LDV on unconstrained structures (such as the hung blade) due to the presence of rigid body modes.
2. The noise-to-signal ratio in LDV is higher and requires additional processing [23, 24].
3. In the substucturing context, the accelerometer sensor mass loading effect can be taken into account in the process with a good degree of accuracy [1, 25].

In order to find out a possible influence of the accelerometers masses on the results of the hybrid model, the case of the disk (Model 2) was reprocessed by keeping into account the accelerometers masses. Assuming that the mounted accelerometers only add inertia on the disk, their mass can either be 1) coupled to the numerical model or 2) decoupled from the experimental FRFs [1]. In the first case, the masses of accelerometers are added to the numerical model of the disk. In the second case, the numerical model does not have the added masses, but the effect must be decoupled from the

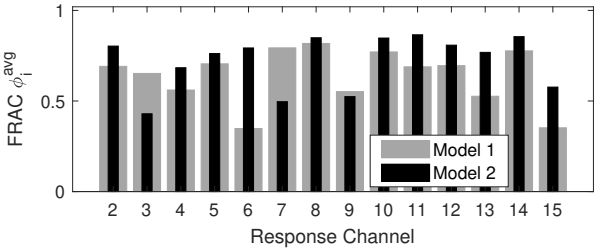

Fig. 13: FRAC bar plot for the disk vs Response Channels. Two different numerical models are used to generate the respective hybrid models and the corresponding correlation levels.

Table 3: OVERALL MEAN FRAC VALUES FOR THE DISK

	Model 1	Model 2	Model 2 with Sensor Mass
With All Channels	0.638	0.719	0.720
Without Channel 3	0.637	0.741	0.742
Without Channel 6	0.660	0.713	0.714

measurements [25–27]. Theoretically, this last choice is possible but practically it needs inversion of the measured FRFs [19, 28], and hence, not preferred.

The first solution was then selected for the present case. There are five accelerometers, as shown in Fig. 11 (the disk on left side), at five different locations, each of them has a nominal mass of 6.5 grams. Therefore, we added a point mass in the numerical Model 2 of the disk at the accelerometer positions. New expanded models were then generated to compute the updated FRAC values. The resulting overall mean FRAC values are listed in the last column of Tab. 3. By comparing the last two columns of the table, it can be noticed that the mean FRAC values are almost unchanged between Model 2 and Model 2 with Sensor Masses. Thus, it can be concluded that the sensor loading has a very little effect on the expanded dynamics of the disk.

5 DISCUSSION

As seen in Section 4, the channels or DoF that were poorly correlated could be easily pointed out by using the simple FRAC correlation. The plots of Fig. 9, Fig. 10 and Fig. 13 can be interpreted alternatively as an indicator of observability and controllability. In a given set of measurements (a posteriori), a measured response channel is predicted by the expansion with all the remaining channels. And by computing the correlation between the two, it is asked if we could observe the same DoF? As noted in Fig. 9, the channel 4 could not be observed by the controls (or inputs) at most of the channels, hence, it was not fully observable with the given set of controls.

The FRAC improvement may seem marginal (about 2 percent points) but it should not be considered so. Even if there

was no overall FRAC improvement, it would mean that the lesser number of channels could observe the same DoF with the same correlation as before. Most importantly, the correlation levels should not drop after an uncorrelated channel was removed.

In the application of the method to the disk –a more complicated test structure– the use of different numerical models demonstrates that even though the overall correlation levels are low, one could still point out the uncorrelated channels depending upon the modal directions of the numerical model. Nonetheless, the closer the numerical model is to the measured model, the better would be the correlation based channels' filtering and the hybrid models.

The method can also be easily applied to identify the uncorrelated input force channels by changing the definition of the overlay models to not include the respective columns.

6 CONCLUSIONS

The paper highlights importance of a set of measurements that can be correlated with a hybrid or expanded model. System Equivalent Model Mixing (SEMM) - a frequency domain expansion method has been used to build hybrid models of a blade and a disk as stand-alone components. In this way, the inaccessible or unmeasurable DoF can be expanded. However, in order to be confident of the expansion from the measurements, a correlation based validation method is proposed. According to the method, from a given set of measurements, overlay models are generated whose dynamics are imposed on the equivalent numerical models. These overlay models are short of one measurement channel each so-called the validation channels. These overlay models are then used to generate the hybrid models which are correlated with the validation channels. The correlation parameter is the Frequency Response Assurance Criteria (FRAC). Using the different hybrid models, it was possible to find the uncorrelated response channel(s). In case of the blade, the numerical and the experimental models were in good agreement and a bad measurement channel could be identified easily.

The method was then applied on a different and more complex system of a disk which had high modal density and a fixed constraint whose numerical and experimental model did not agree well. Two different numerical models were used for this system. The uncorrelated channels for both the models were different and this is in line with the SEMM formulation. That is, the models of the system have to be equivalent, so that the expansion takes place on the same modes of the system. Nevertheless, the removal of uncorrelated channels results in improved correlation at all of the remaining channels. On the same disk component, the accelerometer mass-loading effect was also investigated by coupling their nominal mass to the disk's numerical model. The resulting overall correlations with sensor loading effect were unchanged signifying their negligible effect on the identification of uncorrelated channels.

The new correlated hybrid models of the disk and blade will be used in the next step of the work to identify the joint dynamic properties in the assembled structure.

Acknowledgements

This work is a part of the project EXPERTISE that received funding from the European Union's H2020 research and innovation program under the Marie Skłodowska-Curie grant agreement No 721865.

References

[1] Ewins, D. J., 1995. *Modal Testing: Theory and Practice*, Vol. 108. John Wiley & Sons Inc.

[2] Arras, M., 2016. "On the use of Frequency Response Functions in the finite element model updating". PhD thesis, Sapienza University of Rome.

[3] Herman, A., 1979. "Mass matrix correction using an incomplete set of measured modes". *AIAA Journal,* ***17***(10), pp. 1147–1148.

[4] Baruch, M., 1982. "Optimal correction of mass and stiffness matrices using measured modes". *AIAA Journal,* ***20***(11), pp. 1623–1626.

[5] Dascotte, E., 1991. "Applications of finite element model tuning using experimental modal data". *Journal of Sound and Vibration,* ***25***(6), pp. 22–26.

[6] Chen, J. C., and Garba, J. A., 1980. "Analytical Model Improvement Using Modal Test Results". *AIAA Journal,* ***18***(6), pp. 684–690.

[7] Cottin, N., Felgenhauer, H. P., and Natke, H. G., 1984. "On the parameter identification of elastomechanical systems using input and output residuals". *Ingenieur-Archiv,* ***54***(5), pp. 378–387.

[8] Sestieri, A., and D'Ambrogio, W., 1989. "Why be Modal: How to Avoid the Use of Modes in the Modification of Vibrating Systems". In Proc of the 7th Intl Modal Anal Con, Vol. 25-30, pp. 25–30.

[9] O'Callahan, J., 1989. "System equivalent reduction expansion process (SEREP)". In 7th International Modal Analysis Conference, Society for Experimental Mechanics, Bethel, CT, pp. 29–37.

[10] Thibault, L., Butland, A., and Avitabile, P., 2012. "Variability Improvement of Key Inaccurate Node Groups – VIKING". Springer, New York, NY, pp. 603–624.

[11] Klaassen, S. W., van der Seijs, M. V., and de Klerk, D., 2018. "System equivalent model mixing". *Mechanical Systems and Signal Processing,* ***105***(December), pp. 90–112.

[12] De Klerk, D., Rixen, D. J., and De Jong, J., 2006. "The Frequency Based Substructuring (FBS) method reformulated according to the dual Domain Decomposition method". In Conference Proceedings of the Society for Experimental Mechanics Series.

[13] Heylen, W., and Lammens, S., 1996. "FRAC: A Consistent way of Comparing Frequency Response Functions". In Proceedings, International Conference on Identification in Engineering, Swansea, pp. 48–57.

[14] Grafe, H., 1998. "Model Updating of Large Structural Dynamics Models Using Measured Response Functions". PhD thesis, Imperial College of Science, Technology and Medicine University of London.

[15] Ewins, D. J., 2000. "Model validation: correlation for updating". In Sadhana - Academy Proceedings in Engineering Sciences, Vol. 25, pp. 221–234.

[16] Saeed, Z., Firrone, C. M., and Berruti, T. M., 2019. "Substructuring for Contact Parameters Identification in Bladed-disks". *Journal of Physics: Conference Series,* ***1264***(1), jul, p. 012037.

[17] Saeed, Z., Klaassen, S. W. B., Firrone, C. M., Berruti, T. M., and Rixen, D. J., 2019. "Joint Identification in Bladed-disks using SEMM and VPT". In Tribomechadynamics, M. Brake, ed.

[18] Saeed, Z., Klaassen, S. W. B., Firrone, C. M., Berruti, T. M., and Rixen, D. J., 2020. "Experimental Joint Identification Using System Equivalent Model Mixing in a Bladed Disk". *Journal of Vibration and Acoustics,* ***142***(5), jun.

[19] De Klerk, D., Rixen, D. J., and Voormeeren, S. N., 2008. "General framework for dynamic substructuring: History, review, and classification of techniques". *AIAA Journal,* ***46***(5), pp. 1169–1181.

[20] Klaassen, S. W., 2017. "Towards Hybrid Modular Design of Structural Dynamic Models". PhD thesis, Delft University of Technology.

[21] Smith, S., Bilbao-Ludena, J. C., Catalfamo, S., Brake, M. R., Reuß, P., and Schwingshackl, C. W., 2016. "The effects of boundary conditions, measurement techniques, and excitation type on measurements of the properties of mechanical joints". In *Nonlinear Dynamics, Conference Proceedings of the Society for Experimental Mechanics Series*, G. Kerschen, ed., Vol. 1. Springer, Cham, pp. 415–431.

[22] Zanarini, A., 2019. "Full field optical measurements in experimental modal analysis and model updating". *Journal of Sound and Vibration,* ***442***(July 2013), pp. 817–842.

[23] Hasheminejad, N., Vuye, C., Van den bergh, W., Dirckx, J., and Vanlanduit, S., 2018. "A Comparative Study of Laser Doppler Vibrometers for Vibration Measurements on Pavement Materials". *Infrastructures,* ***3***(4), p. 47.

[24] Stanbridge, A. B., Khan, A. Z., and Ewins, D. J., 2000. "Modal testing using impact excitation and a scanning LDV". *Shock and Vibration,* ***7***(2), pp. 91–100.

[25] Cakar, O., and Sanliturk, K. Y., 2005. "Elimination of transducer mass loading effects from frequency response functions". *Mechanical Systems and Signal Processing,* ***19***(1), pp. 87–104.

[26] Bi, S., Ren, J., Wang, W., and Zong, G., 2013. "Elimination of transducer mass loading effects in shaker modal testing". *Mechanical Systems and Signal Processing,* ***38***(2), pp. 265–275.

[27] Ren, J., Wang, J., Zhou, X., and Ting, K. L., 2017. "Correction of multiple transducers masses effects from the measured frfs". In Proceedings of the ASME Design Engineering Technical Conference, Vol. 8.

[28] Voormeeren, S. N., and Rixen, D. J., 2012. "A family of substructure decoupling techniques based on a dual assembly approach". *Mechanical Systems and Signal Processing,* ***27***(1), feb, pp. 379–396.